HEAT TRANSFER IN TURBOCHARGER TURBINES UNDER STEADY, PULSATING AND TRANSIENT CONDITIONS

RD Burke[a*], C Vagg[a], D Chalet[b] and P Chesse[b]

a. Department of Mechanical Engineering, University of Bath, BA2 7AY, Bath, UK

b. LUNAM Université, École Centrale de Nantes, LHEEA UMR CNRS 6598, 1 rue de la Noë, BP 92101, 44321 Nantes Cedex 3, France

*Corresponding Author contact. Email: R.D.Burke@bath.ac.uk, Tel: +441225383481

ABSTRACT

Heat transfer is significant in turbochargers and a number of mathematical models have been proposed to account for the heat transfer, however these have predominantly been validated under steady flow conditions. A variable geometry turbocharger from a 2.2L Diesel engine was studied, both on gas stand and on-engine, under steady and transient conditions. The results showed that heat transfer accounts for at least 20% of total enthalpy change in the turbine and significantly more at lower mechanical powers. A convective heat transfer correlation was derived from experimental measurements to account for heat transfer between the gases and the turbine housing and proved consistent with those published from other researchers. This relationship was subsequently shown to be consistent between engine and gas stand operation: using this correlation in a 1D gas dynamics simulation reduced the turbine outlet temperature error from 33°C to 3°C. Using the model under transient conditions highlighted the effect of housing thermal inertia. The peak transient heat flow was strongly linked to the dynamics of the turbine inlet temperature: for all increases, the peak heat flow was higher than under thermally stable conditions due to colder housing. For all decreases in gas temperature, the peak heat flow was lower and for temperature drops of more than 100°C the heat flow was reversed during the transient.

Keywords: Turbocharger, Heat transfer, Transient, Thermal modelling

1 INTRODUCTION

Turbocharging internal combustion engines is set to increase rapidly as this is a key technology to deliver fuel economy savings for both Diesel and spark ignition engines [1]. Using a compressor to provide higher air flows to an internal combustion engine increases the power density and allows smaller engines to be used in more high power applications, reducing overall weight and friction. The matching of a turbocharger with an internal combustion engine is a crucial step in the development process and relies on simulation of the engine air path system. In these models, turbochargers are represented by characteristic maps, which are defined from measurements of pressure ratio, shaft speed, mass flow and isentropic efficiency taken from a gas stand. Whilst the mass flow, pressure ratio, and speed can be measured directly, the efficiency has to be calculated from measured gas temperatures. For both turbine and compressor, enthalpy changes in the working fluids are equated to work changes during the characterisation process[1]. Any heat transfer affecting these gas temperature measurements will cause errors in the characterisation process. Conversely, when the characteristic maps are subsequently used in engine simulations to predict engine performance; if heat transfers are ignored then a poor prediction of gas temperatures for inter-cooling and after-treatment will arise. Consequently there is a two-fold interest in understanding and modelling heat transfer in turbochargers:

1. To improve the accuracy of work transfer measurements during characterisation.
2. To improve the prediction of gas temperatures in engine simulations.

Current practice ignores heat transfers and limits investigations to operating conditions where heat transfer are small compared to work transfers; these conditions prevail for the compressor at higher turbocharger speeds but heat transfer is always significant in the turbine. Parametric curve fitting techniques are then used to extrapolate to the lower speed region [2].

[1] Some specialist facilities use a turbine dynamometer to measure turbine work directly, however these rarely used for automotive turbochargers in industrial applications.

This work focuses on heat transfer in the turbine which represents the principal heat source for turbocharger heat transfer and strongly affects the gas temperature entering after-treatment systems. In particular, this paper aims to assess the applicability of gas-stand derived heat transfer models to on-engine conditions where flows are hotter, pulsating and highly transient.

2 BACKGROUND

A number of studies into heat transfer in turbochargers have been presented over the past 15 years. The first studies focussed on quantifying the effects of heat transfer on steady flow gas stands by comparing the work transfers that would be measured based on temperature changes for different turbine inlet temperatures [3-8]. Cormerais et al. [4] presented the most extreme changes in operating conditions, varying turbine inlet temperature from 50°C to 500°C with a thermally insulated turbocharger and observed up to 15%points change in apparent compressor efficiency . Baines et al. [7] measured losses of 700W at 250°C turbine inlet gas temperature (TIT) which is considerably lower than the 2.7kW measured for a similar turbocharger by Aghaali and Angstrom with turbine inlet temperatures ranging 620-850°C [8]. Baines et al. [7] also estimated heat transfer to ambient as 25% of total turbine heat transfer, however at 700°C TIT, where temperature gradients to ambient were much higher, Shaaban [5] estimated this at 70%.

A number of modelling approaches have been used ranging from 3D conjugate heat transfer, giving a detailed insight to the heat transfer processes [9, 10], to simple 1D models for use with engine simulations. The most basic approach adopted to improve the correlation of engine models to experimental data consists of empirically adapting or *correcting* turbine maps using efficiency multipliers [8, 11]. This approach is typically parameterized to estimate heat energy directly using an exponential function that decays with increasing mass flow or turbine power and is tuned to match measured data from an engine or vehicle dynamometer. Whilst this approach can improve the accuracy of engine models, it is not predictive and alternative models have been proposed.

In practice heat transfer will occur through the turbocharger stage [12], however a common assumption in 1D models assumes that heat transfer and work transfer occur independently [13-15]; this is represented schematically on enthalpy-entropy diagrams in figure 1. The actual processes undergone by the gases are shown between states 1-2 and 3-4 for compressor and turbine respectively. The split of work and heat transfer is shown by the intermediate states 1′, 2′, 3′ and 4′ such that flow through the turbine is composed of the following stages:

1. A heating or cooling at constant pressure (processes 1-1′ and 3′-3),
2. An adiabatic compression/expansion (processes 1′-2′ and 3′-4′)
3. A heating or cooling at constant pressure (processes 2′-2 and 4′-4)

Based on this analysis it is obvious that any measurement of temperature change across the turbine or compressor will include both the work and heat transfers, and that any estimate of work based on the total enthalpy change will include an error equal to the net heat transfer (equation 1).

$$\Delta \mathrm{h}_{act} = \Delta \mathrm{h}_{work} + q_b + q_a \qquad (1)$$

The isentropic efficiencies used in engine simulation codes are described for compressor and turbine in equations 2 and 3 respectively. These equations describe the transitions between 1′-2′ and 3′-4′.

$$\eta_{s,c} = \frac{\Delta \mathrm{h}_{s'}}{\Delta \mathrm{h}_{work,c}} = \frac{c_{p,c}\left[T_{01'}\left(\left(\frac{P_{02}}{P_{01}}\right)^{\frac{\gamma-1}{\gamma}} - 1\right)\right]}{\Delta h_{act,c} - q_{b,c} - q_{a,c}} \qquad (2)$$

$$\eta_{s,t} = \frac{\Delta \mathrm{h}_{work,t}}{\Delta \mathrm{h}_{s',t}} = \frac{\Delta h_{act,t} - q_{b,t} - q_{a,t}}{c_{p,t}\left[T_{03'}\left(1 - \left(\frac{P_4}{P_{03}}\right)^{\frac{\gamma-1}{\gamma}}\right)\right]} \qquad (3)$$

In equations 2 and 3 it is common to define efficiencies using total conditions at points 1, 2 and 3 (and hence 1′, 2′ and 3′) and static conditions at point 4 (and 4′). For clarity, these distinctions have been omitted from figure 1.

The major issue that arises in applying equations 2 and 3 is that it is not possible to directly measure $T_{1'}$ $T_{2'}$, $T_{3'}$ and $T_{4'}$ because they are not well defined spatially within the turbocharger. Consequently, for industrial mapping, operation is assumed to be adiabatic, i.e. q_a=q_b=0, T_1=$T_{1'}$; T_2=$T_{2'}$, T_3=$T_{3'}$ and T_4=$T_{4'}$. This assumption holds for a compressor operating at higher shaft speeds where the heat transfer is small compared to the work transfer [16]. On the turbine side, the condition of adiabatic operation can only be achieved in special laboratory conditions and commonly turbine work is estimated either through compressor enthalpy rise or using a turbine dynamometer [17].

The 3D conjugate heat transfer modelling undertaken by Bohn et al [9] showed that heat transfers between the working fluids and the housing could occur in either direction and could change direction as the flow passed through the rotor and diffuser depending on the magnitude of temperature change due to compression or expansion. To capture this in a simplified model, the full problem described by figure 1 should be considered where heat transfers can occur both before and after the compression and expansion processes. However, most authors [14, 18, 19] prefer to group all heat transfers after the compression in the compressor or before the expansion in the turbine: i.e. in figure 1 (a) $q_b = 0$ and in figure 1 (b) $q_a = 0$. This simpler approach stems from a limitation in the parameterisation method. This is performed either by comparing hot operation of the turbocharger with special conditions where temperature gradients are minimised by matching T_2 and T_3[2], or by using the turbocharger bearing housing as a heat flux probe [15]. In both cases further assumptions are required for separating the heat flows before and after work transfers [20] and these are deemed not to provide any further accuracy benefits over lumping all heat transfers into a single process. The convective heat transfer between the working fluid and the housing within the turbine

[2] The turbocharger cooling fluids (oil and water if present) are also matched to the compressor outlet and turbine inlet gas temperatures.

and compressor housing is always modelled by assuming or adapting convective correlations for flows in pipes such as Dittus-Boelter or Seider-Tate [21]. A number of correlations proposed in the literature are presented in table 1. It is difficult to compare these correlations in equation forms because of differences in defining the characteristic lengths. Therefore a graphical representation is given in the results section of this paper (figure 12).

Table 1: Comparison of internal convective heat transfer correlations for turbines

Authors	Source	Correlation	Characteristic Length	Constants		
				a	b	c
Baines et al. [7]	Gas stand	$Nu = aRe^b Pr^c$	L_{volute}	0.032	0.7	0.43
Cormerais [18]			D_{inlet}	0.14	0.75	1/3
Reyes-Belmonte [22]	Gas Stand	$Nu = aRe^b Pr^{1/3} \left(\frac{\mu_{bulk}}{\mu_{skin}}\right)^{0.14} F$ where $F = 1 + 0.9756\left(\frac{\frac{D_{inlet}}{\eta_{max}}}{\frac{(L_{volute})^2}{4D_{inlet}}}\right)^{0.76}$	$\frac{(L_{volute})^2}{4D_{inlet}}$	1.07	0.57	1/3
				5.34	0.48	1/3
				0.101	0.84	1/3
Romagnoli and Martinez-Botas [19]	Theory	$Nu = aRe^b Pr^c$	$\frac{D_{inlet}}{2}$	0.046	0.8	0.4

The heat transfer models have been shown to improve the accuracy of turbine outlet temperature prediction from an over prediction of 20-40°C to within ±10°C [16]. However, no direct comparison has been made for the same device between gas stand and engine operation. In this paper, an investigation with the same turbocharger and crucially the same instrumentation was conducted in both environments.

3 MODELLING AND DATA ANALYSIS

3.1 Total Heat Transfer

An overview of the heat and work flows inside the turbocharger is shown in figure 2. By applying the conservation of energy, the change in enthalpy in the turbine can be related to the work and heat transfer rates using equation 4, with T_{0i} the stagnation or total temperatures.

$$\dot{W}_t + \dot{Q}_{b,t} + \dot{Q}_{a,t} = \dot{m}_t c_{p,t}(T_{03} - T_{04}) \tag{4}$$

Where the turbine work transfer rate can be derived from a power balance on the shaft (equation 5).

$$\dot{W}_t = \dot{W}_c + \dot{W}_f \tag{5}$$

The compressor work transfer rate is estimated using equation 6; this effectively ignores heat transfers on the compressor side. This will cause errors, notably at low speeds and a full analysis of the uncertainties caused by this assumption are given in section 4.4. The friction work was estimated using the model developed by Serrano et al [23] , summarized by equation 7.

$$\dot{W}_c = \dot{m}_c c_{p,c}(T_{02} - T_{01}) \tag{6}$$

$$\dot{W}_f = C_{fr} {N_t}^2 \tag{7}$$

Combining equations 4 with equations 5-7 and rearranging yields the expression for total heat transfer from the gas to turbine housing:

$$\begin{aligned}\dot{Q}_{G/T} = \dot{Q}_{b,t} + \dot{Q}_{a,t} \\ &= \dot{m}_t c_{p,t}(T_{03} - T_{04}) - C_{fr} {N_t}^2 \\ &- \dot{m}_c c_{p,c}(T_{02} - T_{01})\end{aligned} \tag{8}$$

3.2 Heat Transfer model

A simplified heat transfer model was used based on similar approaches found in the literature [4,5,7,13,14,19] (figure 2). The model combines two thermal nodes (compressor and turbine housing), linked via conduction through the bearing housing. Heat transfer between the gases and housings can occur both before and after the compression/expansion processes which is important because of the different temperature gradients between gas and wall.

The focus of this paper remains on the heat transfer between the exhaust gases and the turbine node. Undertaking an energy balance on this node yields equation 9; the heat transfer model aims to determine each of the terms on the right hand side.

$$m_T c_{p,T} \frac{dT_T}{dt} = \dot{Q}_{b,T} + \dot{Q}_{a,T} - \dot{Q}_{T/B} - \dot{Q}_{T,rad} - \dot{Q}_{T,conv} \qquad \mathbf{9}$$

To eliminate $\dot{Q}_{T,rad}$ and $\dot{Q}_{T,conv}$ from equation 9, a measured turbine housing temperature was used which avoids the uncertainties in modelling external heat transfer, most notably with respect to external air flows which strongly affect the convection term [24], are highly specific to different installations (gas stand, engine dynamometer, in-vehicle) and difficult to capture without a full 3D simulation.

The flow path inside the turbine is highly complex with variations in section, flow rates and convective area. For the turbine, the tongue could be approximated to a short pipe of constant diameter, however the scroll has a gradually reducing diameter and mass flow rate as gas enters the stator and rotor flow passages. The flow is then combined in the diffuser, which may once again be approximated as constant diameter pipe. From a heat transfer perspective, this means that the large spatial variations in flow conditions will result in a wide range of local Reynolds numbers that would be difficult to validate experimentally.

In this simplified model, the turbine is considered as two pipes of constant diameter, with an adiabatic expansion between them. The heat transfer in the pipes is calculated using Newton's law of cooling (equations 10 and 11). The total wetted area, $\left(A_T = A_{b,T} + A_{a,T}\right)$ can be determined from part geometry. The breakdown of area pre- and post- compression in this paper is assumed to be 85% of total area before expansion and 15% after, which has been determined based on a qualitative assessment of static temperature drop through the turbine. Whilst a more rigourous approach to determining this breakdown in area could be desirable, previous work on heat flows in compressor housings showed that this breakdown in heat flow only becomes significant if there are large pressure changes in the device [20]. Therefore the arbitrary assignment of distribution in this work is deemed sufficient. Heat flows presented in the subsequent sections of this work consider the total heat transfer over the complete turbine. In this way a spatially averaged Reynolds number is defined for the whole turbine stage, acting over the total heat transfer area. To account for the geometry of the device, the constants a_1 and a_2 of the Seider-Tate convection correlation (equation 12) [21, 25] were determined empirically based on measured gas and wall temperatures.

$$\dot{Q}_{b,T} = h_{b,T} A_{b,T} (T_3 - T_T) \qquad \mathbf{10}$$

$$\dot{Q}_{a,T} = h_{a,T} A_{a,T} (T_{4'} - T_T) \qquad \mathbf{11}$$

with $A_T = A_{a,T} + A_{b,T}$

$$Nu_t = \frac{h_{x,T} D_{T,inlet}}{k_G} = c_1 Re_t^{c_2} Pr^{1/3} \left(\frac{\mu_{bulk}}{\mu_{skin}}\right)^{0.14} \qquad \mathbf{12}$$

It is vitally important the definition of characteristic length D_T and effective heat transfer area $A_{x,T}$ be provided with the convection correlation parameters c_1 and c_2 in equation 12 as many dimensions could be considered for this. Here, the inlet and outlet diameters are defined as characteristic lengths whilst the internal heat transfer area is the total area as calculated from part geometry.

3.3 Work transfer and Gas Dynamic Model

The model assumes that work and heat transfer occur independently. The enthalpy change due to heat transfer is captured by the model described above whilst the work transfer will be captured by an isentropic efficiency term that represents the isentropic efficiency that would be observed experimentally if no heat transfer were present. These were derived from the isentropic efficiencies derived from the gas stand measurements, $\eta_{gas\ stand}$ (equation 13).

$$\eta_{gas\ stand} = \frac{T_{02} - T_{01}}{T_{03} - T_{4s}} \quad (13)$$

However this efficiency term will not account for mechanical losses in the turbocharger bearing as it is based on the apparent work transfer in the compressor. Mechanical losses were estimated using the friction model developed by Serrano et al. [23] (see equation 7). Equation 14 then uses this estimate and the compressor work (equation 6) to calculate mechanical efficiency.

$$\eta_{mech} = \frac{\dot{W}_c}{\dot{W}_f + \dot{W}_c} \quad (14)$$

Equation 15 can then be used to calculate an actual turbine efficiency.

$$\eta_s = \frac{\eta_{gas\ stand}}{\eta_{mech}} \quad (15)$$

To account for the behaviour of the turbine under pulsating flow conditions such as those observed on-engine, a mean line turbine model was used [26]. This represents the turbine as a series of two orifices and an internal volume and was used to calculate instantaneous Reynolds numbers from pulsating pressure measurements.

4 EXPERIMENTAL APPROACH

4.1 Turbocharger description

The turbocharger used in this study was from a 2.2L automotive Diesel engine, with turbine and compressor wheel diameters of 43mm and 49mm respectively. The turbine side included variable guide vanes and cooling was provided by engine lubricating oil.

K-type thermocouples were installed to measure fluid and metal temperatures. At each gas inlet and outlet port, three thermocouples were installed with 0.5, 0.3 and 0.15 diameter protrusions into the flow (figure 3a). These depths were chosen arbitrarily to give a radial temperature distribution. The number of sensors that could be installed was limited by space constraints within the engine components while a greater number of sensors would improve the knowledge of temperature distribution. The sensors were installed through the housing of the turbocharger and therefore as close as possible to the compression and expansion processes thus minimising heat losses between the measurements. In this way, a distribution of temperature is captured at the four gas ports of the turbocharger and is able to capture to a degree the non-homogeneous temperature that exists at these ports [26]. Crucially the instrumentation between gas stand and on-engine remains constant allowing for direct comparison between the two configurations. Additional thermocouples were installed in the bearing, turbine and compressor housings in order to estimate a bulk metal temperature (figure 3b and c).

4.2 Gas stand test facility

A schematic of the gas stand facility is given in figure 4: the turbine is supplied with hot compressed air from a screw compressor and electrical heating system. The flow through the turbine is controlled through an electric valve and measured using a thermal flow meter before being thermally conditioned by two electric heaters. The turbine drives the compressor and flow through the compressor is controlled by a second electric valve, and measured using a second thermal flow meter. Temperatures and pressures are measured at the inlet and outlet of both devices using k-type thermocouples and piezo-resistive sensors respectively. Additional k-type temperature sensors integral to the gas stand facility were also available for these experiments. The turbocharger is lubricated using a dedicated oil supply and conditioning system, ensuring oil temperature remains above 70^{o}C during all experiments.

Turbine maps were measured under thermally stable conditions for two turbine inlet temperatures (100^{o}C and 500^{o}C) and three variable geometry turbine (VGT) positions (20%, 50% and 80%). The operating points are shown on the compressor and turbine maps in figure 5. Corrected flow conditions for compressor and turbine were obtained from equations 16 and 17 respectivly.

$$\dot{m}_{c,corr} = \dot{m}_c \frac{\sqrt{\frac{T_{01}}{298}}}{\frac{P_{01}}{1}} \qquad \mathbf{16}$$

$$\dot{m}_{t,corr} = \dot{m}_t \frac{\sqrt{\frac{T_{02}}{288}}}{\frac{P_{03}}{1.01325}} \qquad \mathbf{17}$$

4.3 Engine test facility

A 2.2L Diesel engine was installed on a transient AC dynamometer and was used to control turbocharger operating point by varying speed and load conditions. The air flow through the compressor was measured directly using an *ABB Sensyflow* hot wire flow meter. The flow through the turbine was estimated from the compressor air flow and the fuel flow, measured from a *CP Engineering FMS1000* gravimetric fuel balance. Pressure measurements were made on a 10Hz basis using *Druck PTX* sensors at the inlet and outlet of both turbine and compressor. At the inlet and outlet of the turbine pressures were also measured on an engine crank angle basis using *Kistler 4049* piezo-resistive sensors.

The following experiments were repeated three times to increase confidence in results:

- 14 thermally stable conditions following 8min stabilisation period (figure 6a)

- Transient step experiments (series of step changes in engine operating point with three minute hold time (see figure 6b). Three minutes was chosen as this allows for the system to stabilise between transients thus allowing for the individual analysis of each step transient.

The steady and transient engine operating conditions are also shown on the turbine and compressor maps in figure 5.

4.4 Measurement Uncertainty

Measurement uncertainty has been carried out for total heat transfer and convection coefficients. This combines uncertainty of individual measurement instruments (see table 2) into the calculated values used in the results section using equation 18 [28].

$$u_y = \left(\sum_{i=1}^{n} \left(\frac{\partial y}{\partial x_i} u_{x_i} \right)^2 \right)^{0.5} \qquad \mathbf{18}$$

As an example, applying equation 18 to equation 4 for the uncertainty of the heat transferred from gas to turbine casing yields:

$$u_{Q_{G/T}} = \begin{pmatrix} \left(\dot{m}_t c_{p,T} u_{T_{03}}\right)^2 + \left(-\dot{m}_t c_{p,T} u_{T_4}\right)^2 \\ +\left(c_{p,t}(T_{03} - T_{04}) u_{\dot{m}_t}\right)^2 \\ +\left(\dot{m}_t (T_{03} - T_{04}) u_{c_{p,t}}\right)^2 \\ +\left(-u_{W_t}\right)^2 \end{pmatrix}^{0.5} \qquad \mathbf{19}$$

Where the uncertainty in the work transfer, u_{WT}, is estimated in a similar manner by applying equation 18 to equations 5-7. Uncertainties arising solely as a result of sensor uncertainties are given as the solid square points in the upper graphs of figure 7 (a-c) for turbine work, turbine heat transfer rate and turbine Nusselt number. The uncertainty for turbine work increases at lower turbine speeds because the measurement is dependent on the difference in temperatures before and after the compressor: as the speed and power reduce, this difference becomes considerably small. In contrast, heat transfer rate and Nusselt number have increasing uncertainties at higher shaft speeds. This is because the uncertainties for both these quantities is highly sensitive to mass flow rate and therefore higher uncertainty results at higher mass flows.

Table 2: Measurement accuracy of various quantities measured on the gas stand/engine stand

Measurement	Unit	Sensor	Accuracy
Temperature	°C	k-type thermocouple	+/-2°C
Air Mass flow	kg/h	ABB Sensyflow	<1%
Pressure	kPa	Piezo-resistive	+/-0.04%

In addition to the measurement uncertainty, of particular importance is the calculation of compressor work based on the temperature measurements at compressor inlet and outlet (equation 6). As stated, this approach ignores heat transfer effects in the compressor for the determination of heat transfer in the turbine. To quantify the uncertainty in the proposed approach, it will be assumed that the magnitude of heat transfer rate in the compressor is similar to that presented by Serrano et al [16]: the ratio of heat transfer rate to total enthalpy rate change in the compressor was presented as a function of total enthalpy rate change in the turbine (equation 20). The estimated compressor heat transfer is directly equated to an additional uncertainty source for compressor work equation 21).

$$\frac{\dot{Q}_c}{\Delta\dot{H}_c} = f(\Delta\dot{H}_t) \quad (20)$$

$$u_{W_c,HT} = \dot{Q}_c \quad (21)$$

The uncertainty due to heat transfer is combined with the sensor uncertainties to calculate the influence on key uncertainties using equation 18. These are presented alongside the sensor only uncertainties in figure 7. For turbine work, the increased uncertainty as a result of ignoring heat transfer is significant for turbocharger speeds below 100krpm and at 50krpm the increased uncertainty through ignoring heat transfer is around 30% of the measured value. Clearly this is a severe limitation and illustrates why turbine maps measured in this way are only provided at higher shaft speeds. The effect on uncertainty for turbine heat transfer and Nusselt number is considerably less and at 50krpm the uncertainty increase is only 6% of the measurement. It is these latter two quantities that are most important and high uncertainties for the turbine work will be tolerated.

5 RESULTS AND DISCUSSION

5.1 Overview of Heat transfer

The ratio of heat to work transfer gives an indication of the importance of heat transfer for turbine performance prediction. This is shown over the engine operating map in figure 8, against turbine mechanical power in figure 9 and over the turbine map in figure 10. This highlights the problem that heat transfer is more significant a lower turbine powers where they are not typically mapped, corresponding to lower engine powers. The results in figures 9 and 10 are obvious because they show that heat transfer is strongly linked to temperature and operating point. It is interesting to note that heat transfer accounts for at least 20% of the enthalpy drop over the turbine but that at low turbine powers, this proportion can be significantly higher, even with low turbine gas temperatures. Through figure 9, the exponential correction curves used to correct turbine maps for correlating engine models to measured data [8, 11] are clearly visible.

5.2 Internal Convection

5.2.1 Steady Flow Results

Measured Reynolds and Nusselt numbers are plotted for different VGT positions and turbine inlet temperatures in figure 11; 95% confidence intervals are also shown. The results show that the range of Re numbers under cold and hot flow conditions are an order of magnitude different due to changes in density and mass flow. For a turbine inlet temperature of 500^{o}C (figure 11 a), the Nu/Re relationship has a similar shape to the Seider-Tate correlation for straight pipes. There is also very little distinction within the error margins with respect to VGT position. The 95% uncertainty margins are acceptable but grow with increasing Reynolds number. In contrast, at 100^{o}C TIT, (figure 11 b), the measured Nu/Re relationship has an exponential shape and very high uncertainty. This is because the largest uncertainty is associated with the temperature measurements, and the sensitivity of this uncertainty is linked to mass flow (equation 8). As mass flow is higher under colder conditions, the uncertainty is also higher.

The data measured for turbine inlet temperature of 500^{o}C was used to fit coefficients to equation 12. Initially these correlations have been established using the gas stand specific temperature measurements rather than the thermocouples mounted onto the turbocharger as this provided consistency with other published works, assumed to use these emasurements, which allows a direct comparaison. In figure 12, these new convective correlations are compared to the other published correlations previously presented in table 1. Cormerais et al. [18] and Reyes [22] established turbocharger-specific correlations (three different devices for Reyes) resulting in an individual correlation for each device. These devices were of varying size but all aimed at passenger car applications ranging from 1.2 to 2.0L displacement. Baines et al [7] derived a single correlation, validated for three turbochargers of similar size for automotive truck applications (hence larger than those studied by Reyes and Cormerais et al.). In contrast, Romagnoli et al. [19] proposed to use an established correlation for flow in pipes.

It can be seen that the pipe flow correlation (Romagnoli) agrees well with two of the correlations proposed by Reyes (1 and 2). In contrast the Reyes 3 correlation estimates higher convective heat transfer and agrees better with the correlation proposed by Cormerais et al. Baines' correlation sits in between these two extremes. The correlations derived from the present work give a similar magnitude to the correlations from Cormerais and Reyes (3). There is significant variation depending on the VGT guide vane angle which could be expected because of the way these guide vanes will affect the flow characteristics within the volute and wheel. It should be remembered that the coefficients of the correlation are required to capture the complex 3D flow phenomenon occuring within the device. Reyes [22] also observed this influence of VGT with similar magnitudes difference. However, in this study it is observed a gradual decrease with VGT opening, Reyes observed a correlation with peak turbine efficiency, meaning peak convective heat transfer was observed at intermediate VGT vane angles with lower correlations as the vanes were opend or closed.

There are no obvious links between the correlations and the characteristics of each of the turbochargers based on the available data.

1. When considering the size of the different turbochargers, the correlations proposed by Reyes [22] rank with device size, with Reyes 1 the largest (from 2.0L engine) and Reyes 3 smallest from a 1.2L engine. However the correlation proposed by Baines [7] is for considerably larger commercial vehicles and the device used in the present paper is taken from a 2.2L engine.
2. When considering the inclusion of variable geometry guide vanes, the turbochargers used to derive correlations Reyes 1 and 2, Cormerais and those from the present paper were all fitted with the VGT devices and span the full range of observed convective heat transfer.

The wide range of values proposed in the literature show that it is not yet possible to derive a single, simple convective heat transfer correlation applicable across different turbocharger devices. Whilst this highlights the need for further study in this area, for the purpose of the present study it demonstrates consistency with other research findings.

Turbine Nusselt numbers were also calculated based on the gas stand data using the thermocouples located on the turbocharger inlet and outlet port, and identical to the measurements used on-engine. These are compared to those obtained previously and to results from the engine experiments in figure 13. These will be discussed in the next section.

5.2.2 On-engine results

The analysis was repeated for engine based experiments and results are shown in figure 13. To allow direct comparison of engine conditions with exhaust gases and gas stand conditions with air, the results have been adjusted to a Prandtl number of 0.7 using equation 22.

$$Nu_{(Pr=0.7)} = Nu_{(Pr=x)} \frac{0.7^{1/3}}{Pr_x^{1/3}} \qquad \mathbf{22}$$

The results in figure 13 shows good agreement between the engine and gas stand data when the same temperature sensors are used in both cases. The agreement is worst when comparing the engine data with that obtained from the gas stand using gas stand standard instrumentation, especially at low Reynolds numbers. The discrepancy between gas stand and engine Nusselt number at low Reynolds number can primarily be attributed to the measurements of temperatures at inlet and outlet of the turbine. On the gas stand, conditions for this measurement are more favourable as the flow is both steady and enters and leaves the turbine long straight pipes. On the engine, the flows are both pulsating and the geometry of the exhaust manifold and subsequent exhaust system make the temperature measurement particularly complex. Future studies should consider further measures to promote the accuracy in an engine situation such as the inclusion of bespoke measurement sections replicating to some extent the gas stand layout. It is interesting to note that when using the same instrumentation on-engine and on gas stand, there is strong agreement despite the differences in flow conditions showing that sensor location is a dominant effect.

Using the gas-stand derived correlation with standard instrumentation to predict the turbine outlet temperature on-engine, improved turbine outlet temperature prediction as shown in figure 14. This equates to a reduction of mean error from 33^{o}C to -3^{o}C but an increase in standard deviation of error from 10^{o}C to 20^{o}C.

The model was also used to investigate the effect of pulsating flows on the internal convection. Until now, the Re and Nu numbers have been considered both spatially and time averaged. Pulsating flows equate to pulsating Reynolds numbers as illustrated in figure 15 (obtained from the 1D turbine flow model). Figure 16 compared three different Nusselt/Reynolds relationships obtained as follows:

1. Raw Measurement: obtained using the raw measurements of mass flow from the engine test bench (from the intake air flow and fuel flow measurements).
2. Pulsating Simulation: obtained by using a simulated mass flow based obtained by applying measured instantaneous pressure measurements from the turbine inlet and outlet and applying these to a double orifice model proposed by Serrano et al. [26].
3. Arithmetic mean of pulsating simulation: average Nusselt and Reynolds number over two engine revolutions corresponding to four pulsations, one from each of the engine cylinders.

There is a small offset between the arithmetic mean and the point that results from the physical averaging due to slow sensors response. However, as shown in figure 14, this has little effect on the accuracy of turbine outlet temperature prediction.

5.3 Effect of transient operation

The transient events on engine affect the turbocharger at a range of timescales [29]. It has been shown in the previous section that the flow pulsations have only a small impact on the heat transfer phenomenon. This is explained by the large time constant associated with the thermal inertia of the turbine housing compared with the frequency of the exhaust pulsations. Engine transients occur over a longer timescale and the dynamics of heat transfer will become significant as illustrated in figure 17. The figure shows measured turbine inlet temperature and rotational speed and calculated heat flows following two near step changes in engine power. The calculated heat flows are obtained by the heat transfer model whilst applying measured boundary conditions of turbine inlet and outlet pressure, turbine inlet temperature and turbine rotational speed.

Figure 17 (a) illustrates the case of a step up in engine power. Initially the engine is operating under stable conditions: heat flow from gas to the turbine housing almost equals the heat flow out of the housing and the net heat flow into or out of the housing wall (heat storage) is null. The engine undergoes a rapid power transient at time t=0s causing a rise in turbine inlet temperature through higher fuelling levels. Other control actions also occur such as closing of variable geometry guide vanes. The turbine rotation speed increases sharply over the next 5 seconds with the dynamics controlled by the mechanical inertia of the shaft and loadings on the compressor. The measured turbine inlet temperature undergoes two distinct phases: over the first 30s the temperature rise is relatively large, increasing from 320^{o}C to 474^{o}C. The temperature overshot in this period can be explained by a particular transient characteristic of the engine control which allows a temporary overboosting of the engine. From 30s to 150s after the change in engine power, the temperature rise is much slower with an increase to 492^{o}C. These temperature measurements, which are also used to calculate the heat flows in figure 17 will be affected by the response of the thermocouples used in the measurement. The response of the thermocouple is dependent on the thermal inertia, and therefore the size of the thermocouples, but also the flow conditions and notably the Reynolds number in the pipe. Analysis presented in appendix 1 for 3mm diameter thermocouples shows that the 95% response time for turbocharger inlet and outlet conditions is in the range of 4-20s. Clearly this will affect the accuracy during the initial rapid response corresponding to the first 30s of the response. However, this will have a much smaller impact on the accuracy of the second phase of the response 30-150s. The heat flow from gas to housing peaks at the beginning of the transient (in this case at around 7kW) before slowly falling to a value of around 3.6kW three minutes later. This spike in heat flow is accounted for by the accumulation of heat in the turbine housing as it warms up.

Figure 17 (b) shows the opposite case for a step down in engine load. The heat loss from the gas to housing has a minimum which, in this particular case, is -200W before tending to around +200W three minutes after the transient. This indicates that the heat flow is reversed just after the transient, flowing from the housing to the gas. The same comments for figure 17 (a) with regard to thermocouple response time equally apply to figure 17 (b).

For a series of steps in engine power of different magnitude, the peak and settled heat transfers have been defined as follows:

- **ΔT_3**: The temperature difference between instances just prior to step change in engine power and three minutes after the step change.
- $\dot{Q}_{Peak}$: Maximum or minimum measured heat flow during first 60s following step change in engine power
- $\dot{Q}_{Settle}$: Mean measured heat flow between 160 and 180 seconds following step change in engine power

The quotient of these two heat flow values have been plotted against step change in turbine inlet temperature in figure 18.

For heat flow between the exhaust gases and the turbine casing, figure 18a shows that larger TIT transients result in larger ratio of initial to settled heat transfer. It is important to bear in mind that Q_{settle} was always a positive, as ultimately the exhaust gases are always hotter than the ambient.

- Points in the upper right quadrant correspond to a positive step in exhaust gas temperature. Every case in this quadrant has a Q_{peak}/Q_{settle} ratio greater than 1 meaning the peak heat flow is larger than the settled flow.
- Points located in the upper left quadrant correspond to step reductions in TIT temperature and all have a Q_{peak}/Q_{settle} value between 0 and 1. These points all correspond to step reductions in exhaust gas temperature of less than 100^{o}C.
- Points located in the lower left quadrant correspond to situations where the peak heat flow is reversed (i.e. from the casing to the exhaust gases). These correspond to larger reductions in TIT of more than 100^{o}C.

Figure 18b shows the same ratio for heat transfer from the turbine housing to its surroundings (ambient and bearing housing). For all steps, positive and negative, of less than 100^{o}C this ratio is approximately equal to 1 meaning there is no significant peak in heat flow. This is because the turbine housing temperature does not change significantly and ambient temperature remains constant, therefore heat transfers with the surroundings are not affected. It is only when much larger step changes in turbine inlet temperature are induced that peak heat flow begins to appear.

6 CONCLUSIONS

In this paper, an experimental and lumped capacity modelling approach was used to assess heat transfer characteristics in turbocharger turbines. Through this work, the following conclusions have been drawn:

1. Heat transfer in the turbine always represents at least 20% of enthalpy change in the turbine, however it can be significantly more under low turbine power conditions. This corresponds to the low power operating conditions of the engine in the low speed/low torque region
2. It is difficult to compare the fitted curves for Nusselt /Reynolds correlations at different turbine inlet temperatures because the Reynolds numbers vary by an order of magnitude due to changes in fluid density. Consequently direct comparison relies on considerable extrapolation away from the measured data.
3. Heat transfer correlations determined on-engine and gas stand can be significantly different due to different instrumentation layouts, however when consistent sensors are used across facilities, good agreement is obtained despite the differences in flow conditions.
4. Despite the discrepancies incurred due to instrumentation differences, the use of heat transfer correlations obtained from the gas stand to simulate on-engine conditions will provide a significant improvement in prediction accuracy using either averaged or pulsating flow Reynolds numbers. This shows quasi-steady behaviour can be assumed for convective

heat transfer coefficient. Care should be taken to account for the change in Prandtl number due to variations in gas composition between air and exhaust gases. Application of the gas stand derived heat transfer correlation reduced the turbine outlet temperature prediction error from 33°C to -3°C.

5. Operation under transient conditions shows that the thermal inertia of the housing significantly influences the heat flow because of the change in temperature difference between gas and wall. For large reductions in turbine inlet temperature (greater than 100°C), the heat flow was reversed during the transient.

7 GLOSSARY

7.1 Nomenclature

A	Area	m^2
c	Empirical Constant	
C_{fr}	Friction Constant	W/rpm^2
c_p	Heat capacity at constant pressure	J/kgK
D	Diameter	m
h	Specific enthalpy,	kJ/kg,
	Convective Heat Transfer coefficient	W/m^2K
k	Thermal Conductivity	W/mK
L	Characteristic length	m
m	Mass	kg
$\dot{m}$	Mass flow	kg/s
N	Shaft Speed	1/min
Nu	Nusselt Number	
P	Pressure	Bar
Pr	Prandtl Number	

q	Specific heat flow	kJ/kg
$\dot{Q}$	Heat transfer rate	W
Re	Reynolds Number	
T	Temperature	K
t	time	s
u	Uncertainty	
v	velocity	m/s
W	Work	J
$\dot{W}$	Work transfer rate	W
x	Length (Conduction)	m
	Independent Variable (uncertainty analysis)	
y	Dependent Variable (uncertainty analysis)	
γ	ratio of specific heats	
η	Efficiency	
μ	Dynamic Viscosity	kg s^{-1} m^{-1}
ρ	Density	Kg/m^3
τ	Thermocouple Time Constant	s

7.2 Subscripts

0	Stagnation (temperature)
1	Pre Compressor
1’	Pre compression
2	Post Compressor
2’	Post Compression
3	Pre Turbine
3’	Pre Expansion

4	Post Turbine
4’	Post Expansion
a	After compression/expansion
act	Actual
b	Before compression/expansion
B	Bearing Housing
bulk	Fluid bulk property
c	Compressor
conv	Convective
corr	Corrected
d	inlet diameter
f	friction
g	Gas
rad	Radiation
s	Isentropic (Efficiency)
skin	Fluid film skin property
t	Turbine
tc	thermocouple
T	Turbine Housing
work	Mechanical Work

7.3 Abbreviations

BMEP	Brake Mean Effective Pressure
CO_2	Carbon Dioxide
EGR	Exhaust Gas Recirculation
RMSE	Root mean square error
TIT	Turbine Inlet Temperature
VGT	Variable Geometry Turbine

8 REFERENCES

[1] Taylor, A.M.K.P., Science review of internal combustion engines, *Energy Policy,* vol. 36, pp. 4657-4667, 2008, DOI: 10.1016/j.enpol.2008.09.001

[2] Moraal, P. and Kolmanovsky, I., Turbocharger Modelling for Automotive Control Applications, SAE Paper Number 1999-01-0908, 1999

[3] Chesse, P., Chalet, D., and Tauzia, X., Impact of the heat transfer on the performance calculations of automotive turbocharger compressor (Influence des transferts thermiques sur le calcul des performances des compresseurs de suralimentation), *Oil and Gas Science and Technology,* vol. 66, pp. 791-800, 2011, DOI: 10.2516/ogst/2011129

[4] Cormerais, M., Hetet, J.F., Chesse, P., and Maiboom, A., Heat Transfer Analysis in a Turbocharger Compressor: Modeling and Experiments, SAE Paper Number 2006-01-0023, 2006, DOI: 10.4271/2006-01-0023

[5] Shaaban, S., Experimental investigation and extended simulation of turbocharger non-adiabatic performance, PhD, Fachbereich Maschinenbau, Universität Hannover, Germany, 2004.

[6] Serrano, J.R., Guardiola, C., Dolz, V., Tiseira, A., and Cervelló, C., Experimental Study of the Turbine Inlet Gas Temperature Influence on Turbocharger Performance, SAE Paper Number 2007-01-1559, 2007, DOI: 10.4271/2007-01-1559

[7] Baines, N., Wygant, K.D., and Dris, A., The analysis of heat transfer in automotive turbochargers, *Journal of Engineering for Gas Turbines and Power,* vol. 132(4), 2010, DOI: 10.1115/1.3204586.

[8] Aghaali, H. and Angstrom, H.-E., Improving Turbocharged Engine Simulation by Including Heat Transfer in the Turbocharger, SAE Paper Number 2013-01-0703, 2012, DOI: 10.4271/2012-01-0703

[9] Bohn, D., Heuer, T., and Kusterer, K., Conjugate flow and heat transfer investigation of a turbo charger, *Journal of Engineering for Gas Turbines and Power,* vol. 127(3), pp. 663-669, 2005, DOI: 10.1115/1.1839919.

[10] Heuer, T. and Engels, B., Numerical analysis of the heat transfer in radial turbine wheels of turbo chargers, *proceedings of the 2007 ASME Turbo Expo,* pp. 959-968, May 14-17, 2007, Montreal, Que., Canada, 2007

[11] Jung M., Ford R.G., Glover K., Collings N., Christen U. and Watts M.J. Parameterization and Transient Validation of a Variable Geometry Turbocharger for Mean-Value Modeling at Low and Medium Speed-Load Points. SAE Paper 2002-01-2729, 2002.

[12] Casey, M.V. and Fesich, T.M., The efficiency of turbocharger compressors with diabatic flows, *Journal of Engineering for Gas Turbines and Power,* vol. 132, 2010, DOI: 10.1115/1.4000300

[13] Cormerais, M., Chesse, P., and Hetet, J.-F., Turbocharger heat transfer modeling under steady and transient conditions, *International Journal of Thermodynamics,* vol. 12, pp. 193-202, 2009, ISSN: 1301-9724

[14] Olmeda, P., Dolz, V., Arnau, F.J., and Reyes-Belmonte, M.A., Determination of heat flows inside turbochargers by means of a one dimensional lumped model, *Mathematical and Computer Modelling,* vol. 57, pp. 1847-1852, 2013, DOI: 10.1016/j.mcm.2011.11.078.

[15] Serrano, J.R., Olmeda, P., Paez, A., and Vidal, F., An experimental procedure to determine heat transfer properties of turbochargers, *Measurement Science & Technology,* vol. 21, Mar 2010, DOI: 10.1088/0957-0233/21/3/035109.

[16] Serrano, J., Olmeda, P., Arnau, F., Reyes-Belmonte, M., and Lefebvre, A., Importance of Heat Transfer Phenomena in Small Turbochargers for Passenger Car Applications, *SAE Int. J. Engines,* vol. 6, pp. 716-728, 2013, DOI: 10.4271/2013-01-0576.

[17] Szymko, S., Mcglashan, N.R., Martinez-Botas, R., and Pullen, K.R., The development of a dynamometer for torque measurement of automotive turbocharger turbines, *Proceedings of*

the Institution of Mechanical Engineers, Part D: Journal of Automobile Engineering, vol. 221, pp. 225-239, 2007, DOI: 10.1243/09544070JAUTO401.

[18] Cormerais, M., Caractérisation expérimentale et modélisation des transferts thermiques au sein d'un turbocompresseur automobile. Application à la simulation du comportement transitoire d'un moteur Diesel à forte puissance spécifique, Thèse de Doctorat, École Doctorale Mecanique, Thermique et Genie Civil, École Centrale de Nantes et Université de Nantes, Nantes, France, 2007.

[19] Romagnoli, A. and Martinez-Botas, R., Heat transfer analysis in a turbocharger turbine: An experimental and computational evaluation, *Applied Thermal Engineering,* vol. 38, pp. 58-77, 2012, DOI: 10.1016/j.applthermaleng.2011.12.022.

[20] Burke R.D., Copeland C.D. and Duda T. Investigation into the Assumptions for Lumped Capacitance Modelling of Turbocharger Heat Transfer. 6th International Conference on Simulation and Testing. Berlin, Germany: Expert-Verlag, 2014.

[21] Incropera, F.P. and De Witt, D.P., *Introduction to Heat transfer*, 2nd ed. New York: John Wiley and sons Inc., ISBN: 0-471-51728-3, 1985.

[22] Reyes-Belmonte M.A. Contribution to the Experimental Characterization and 1-D Modelling of Turbochargers for Ic Engines. Departamento de Máquinas y Motores Térmicos. València: Universitat Politècnica de València, 2013.

[23] Serrano, J.R., Olmeda, P., Tiseira, A., Garcia-Cuevas, L.M., and Lefebvre, A., Theoretical and experimental study of mechanical losses inautomotive turbochargers, *Energy,* vol. 55, pp. 888-898, 2013, DOI: 10.1016/j.energy.2013.04.042.

[24] Payri F., Olmeda P., Arnau F.J., Dombrovsky A. and Smith L. External Heat Losses in Small Turbochargers: Model and Experiments. Energy. 2014; 71: 534-46.

[25] Rohsenow, W.M., Hartnett, J.P., and Cho, Y.I., *Handbook of Heat Transfer*, Third Edition ed. New York: McGraw-Hill, ISBN: 1998

[26] Serrano, J.R., Arnau, F.J., Dolz, V., Tiseira, A., and Cervelló, C., A model of turbocharger radial turbines appropriate to be used in zero- and one-dimensional gas dynamics codes for internal combustion engines modelling, *Energy Conversion and Management,* vol. 49, pp. 3729-3745, 2008, DOI: 10.1016/j.enconman.2008.06.031

[27] Baar R., Biet C., Boxberger V. and Zimmermann R. New Evaluation of Turbocharger Components Based on Turbine Outlet Temperature Measurements in Adiabatic Conditions. IQPC-Tagung DOWNSIZING & TURBOCHARGING. Dusseldorf, Germany2014.

[28] Anon, JCGM 100:2008(E) Guide to the expression of uncertainty in measurement (GUM)*, JCGM,* 2008*,* Available: http://www.iso.org/sites/JCGM/GUM/JCGM100/C045315e-html/C045315e.html?csnumber=50461 (accessed 30/07/2010)

[29] Copeland, C.D., Newton, P., Martinez-Botas, R.F., and Seiler, M., A comparison of timescales within a pulsed flow turbocharger turbine, in *10th International Conference on Turbochargers and Turbocharging,* pp. 389-404, May 15-16, 2012, London, United kingdom, 2012

9 APPENDIX. ESTIMATING THE TRANSIEINT RESPONSE OF THERMOCOUPLE PROBES

In order to estimate the transient response of a thermocouple probe situated in the gas stream at the inlet or outlet of the turbocharger turbine, the problem can be assumed to be equivalent to that of a small sphere located within a flow of gas. The convective heat transfer coefficeint for such a configuration has been determined empirically and can be calculated from equation 23 [21].

$$Nu_{tc} = 2 + \left(0.4\sqrt{Re_{tc}} + 0.06Re_{tc}^{2/3}\right)Pr^{0.4}\left(\frac{\mu_{bulk}}{\mu_{skin}}\right)^{1/4} \tag{23}$$

Where the characteristic length is the diameter of the thermocouple tip d_{tc}.

The main stream velocity at the inlet or outlet of the turbine can be related to the mass flow in the turbine using equation 24. This velocity is then used in the callculation of the Reynolds Number.

$$v = \frac{\dot{m}_t}{\rho_g A} \tag{24}$$

The heat transfer coefficient can then be derived from the Nusselt number and the fluid properties and be used to estimate the heat transfer by convection between the gas and the thermocouple tip using Newton’s law of cooling (equation 25).

$$\dot{Q}_{g\_tc} = h_{tc}A_{tc}\left(T_g - T_{tc}\right) \tag{25}$$

Assuming that heat transfer by convection between the gas and the thermocouple is the only significant heat flow, then this heat transfer can be equated to the temperature rise of the thermocouple tip using equation 26

$$m_{tc}c_{p,tc}dT_{tc} = h_{tc}A_{tc}\left(T_g - T_{tc}\right)dt \tag{26}$$

Equation 26 can be rearranged into equation 27 which defined a one degree of freedom first order system.

$$\frac{m_{tc}c_{p,tc}}{h_{tc}A_{tc}}\frac{dT_{tc}}{dt}+T_{tc}=T_g \qquad \textbf{27}$$

Considering that the system is initially at equilibrium where $T_{tc}=T_g(0)$. At time *t=0*, a step change in gas temperature ΔT_g occurs.The thermocouple response would be given by equation 28.

$$T_{tc}(t)=T_g(0)+\Delta T_g\left(1-e^{-\frac{t}{\tau}}\right) \qquad \textbf{28}$$

Where the time constant $\tau=\frac{m_{tc}c_{p,tc}}{h_{tc}A_{tc}}$

This standard first order system response has a 95% response time of three time constants. This response time is shown for thermocouples of diameter 0.5mm, 1.5mm and 3mm as a function of turbine Reynolds number in figure 19. These have been calculated assuming that the fluid is air at 400°C. It should be noted that this Reynolds number (Re_T) is related to the turbine inlet or outlet diameter and therefore directly comparable to the heat transfer correlations used in this work. This is different to the Reynolds number used in this appendix (Re_{tc}) which is used to determine the heat transfer coefficient to the thermocouple tip. The results show that for a 3mm diameter thermocouple, the 95% response time will vary between 5s at high flow rates to 17s at low flow rates. Variations as a result in the change in fluid properties due to changes in temperature affect these results by aoround 8% per 100°C. This means that for the same 3mm thermocouple, the range of 95% response times at the highest likely turbine inlet temperature of 900°C is 4s to 14s whilst at the lowest likely turbine inlet temperature of 200°C it is 6s to 20s.

It can be concluded from this analysis that the response time of the thermocouples used in this work will be in the region of 4 to 20s.

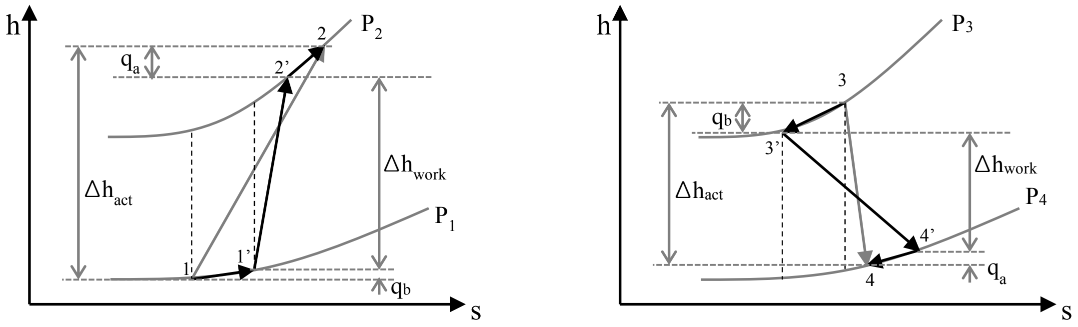

(a) Compressor *(b) Turbine*

Figure 1: Apparent and assumed compression and expansion processes in (a) compressor and (b) turbine

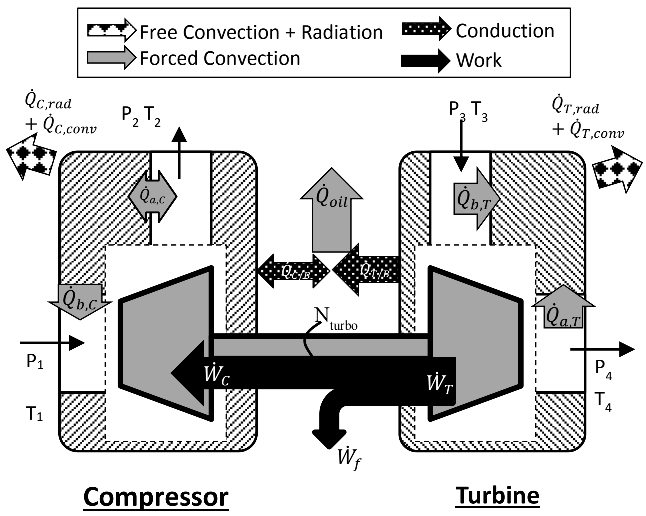

Figure 2: Overview of turbocharger heat transfer model

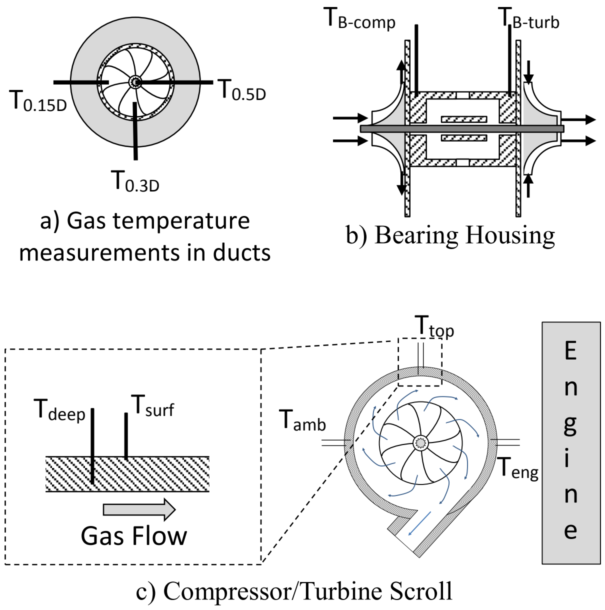

Figure 3: Thermal instrumentation of turbocharger housing and gas ports

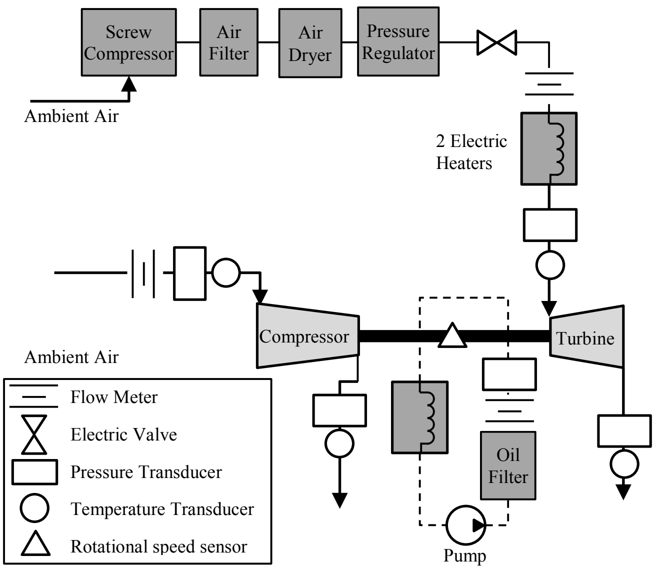

Figure 4: Schematic of gas stand installation

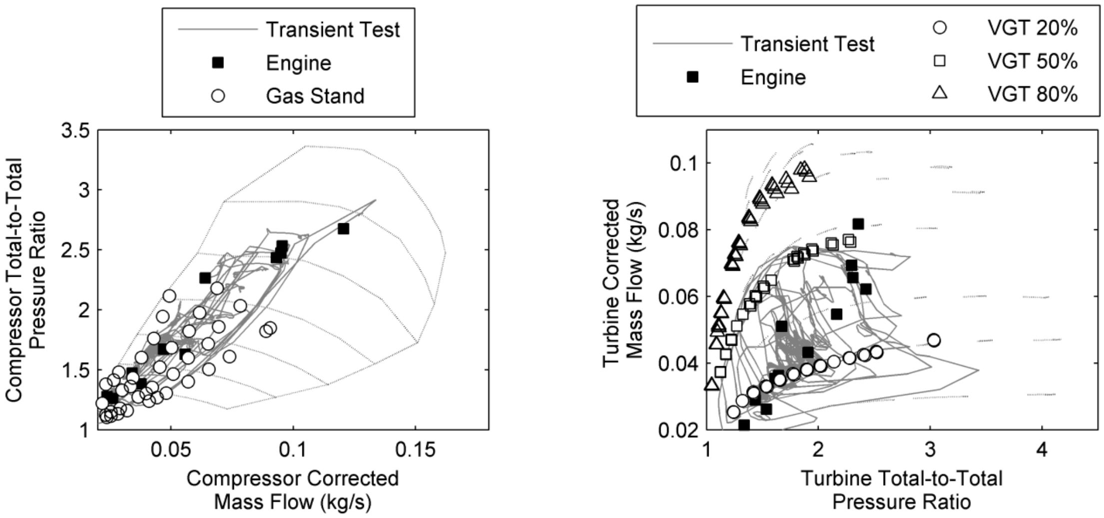

Figure 5: Compressor and Turbine operating points during steady flow gas stand experiments

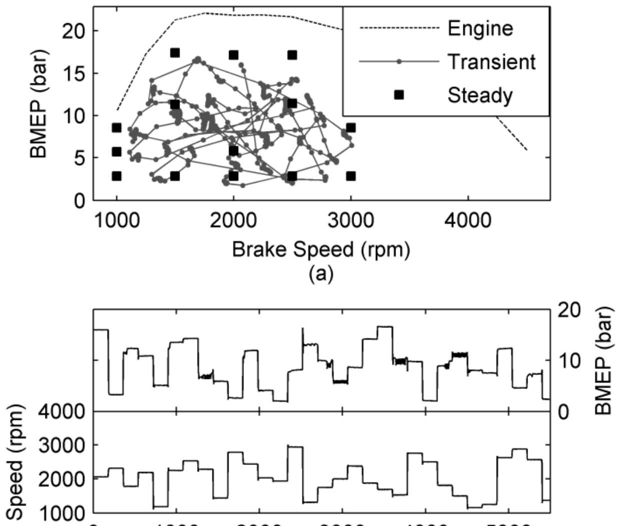

Figure 6: Compressor, Turbine and engine operating points for steady and transient experiments

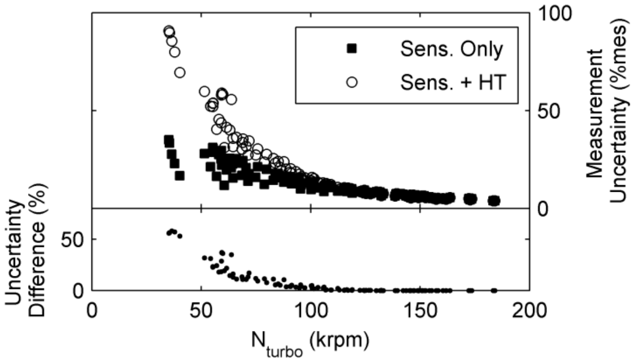

(a) - Turbine Work

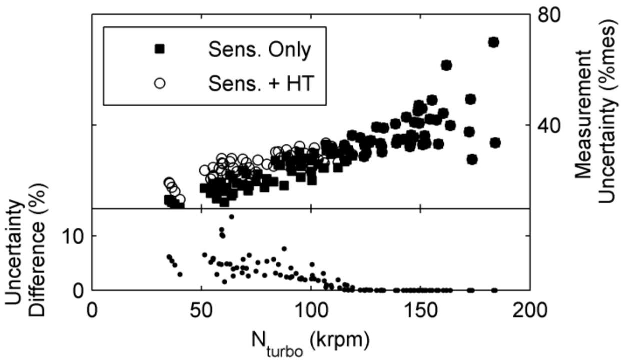

(b) - Turbine Heat Transfer

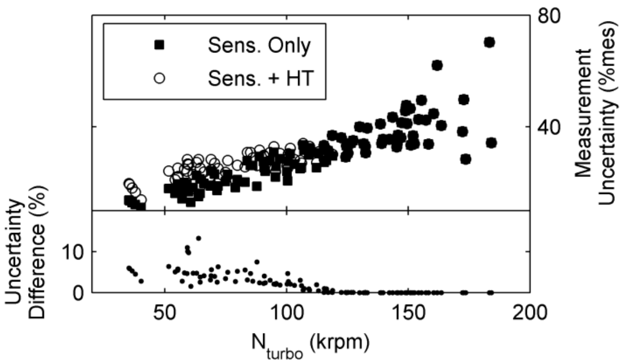

(c) - Turbine Nusselt Number

Figure 7: Estimated combined uncertainty for (a) turbine work transfer rate, (b) turbine heat transfer rate and (c) turbine Nusselt number. Uncertainties due only to sensor uncertainty are compared with uncertainty due to sensors and ignoring heat transfer in the compressor side.

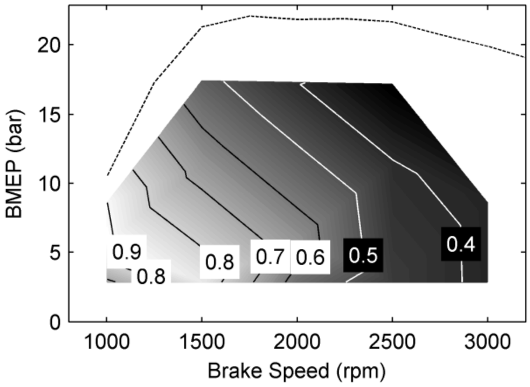

Figure 8: $Q_{G/T}/W_T$ over the engine operating map

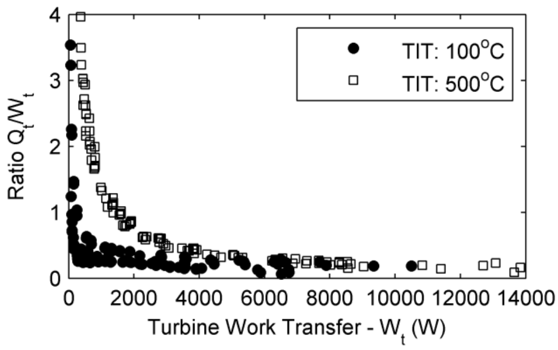

Figure 9: Ratio of turbine total heat loss to turbine work from gas stand testing with TIT 100°C and 500°C

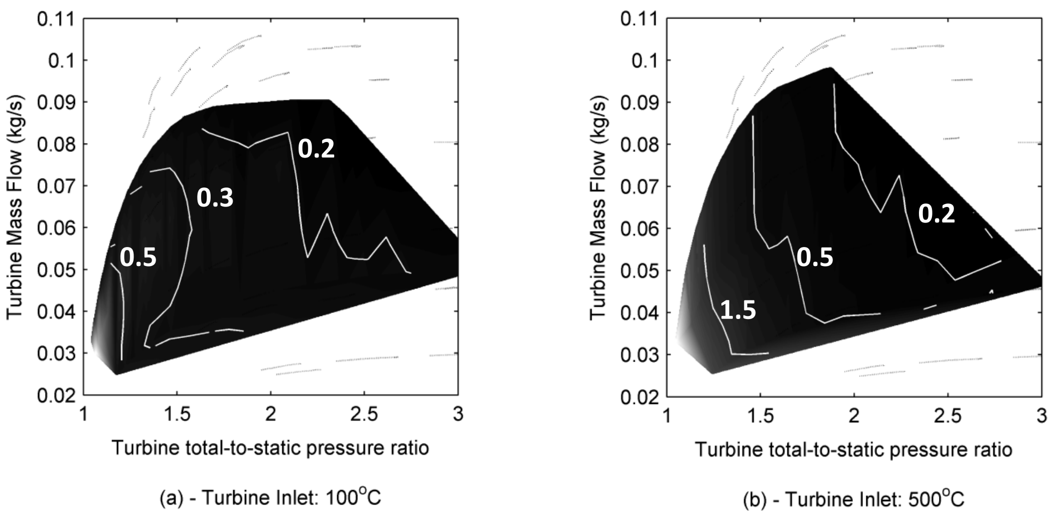

Figure 10: Ratio of turbine total heat loss to turbine work over the turbine operating map for turbine inlet temperature (a) 100°C and (b) 500°C

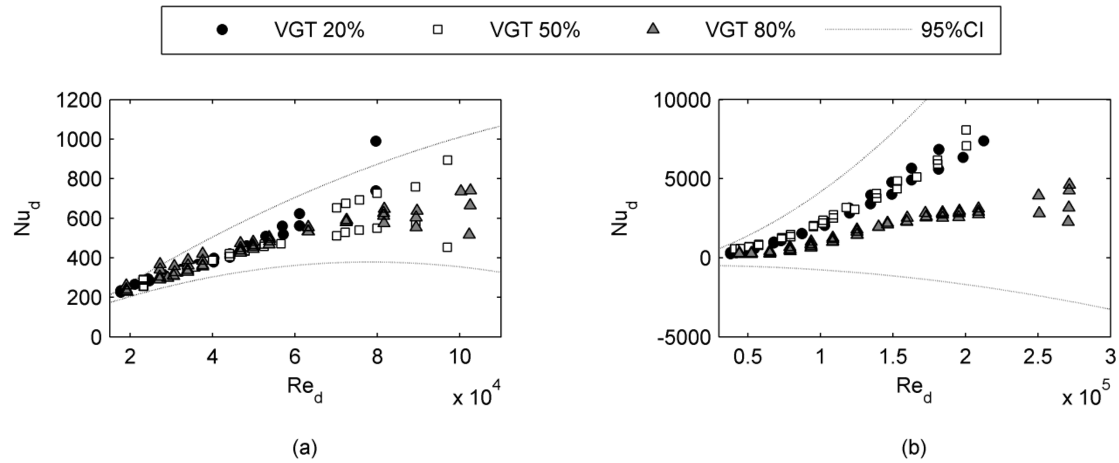

Figure 11: Spatially averaged Nu/Re correlation based on steady flow gas stand experiments for turbine inlet temperature (a) 500°C and (b) 100°C

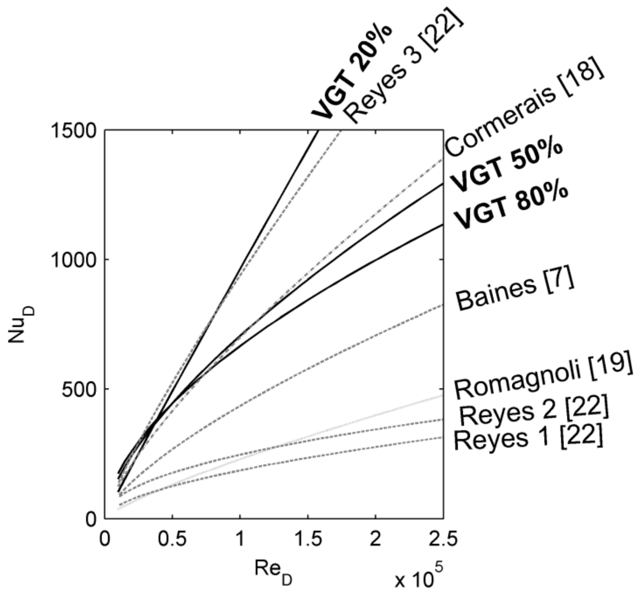

Figure 12: Comparison of fitted convection correlations with selected correlations from published literature

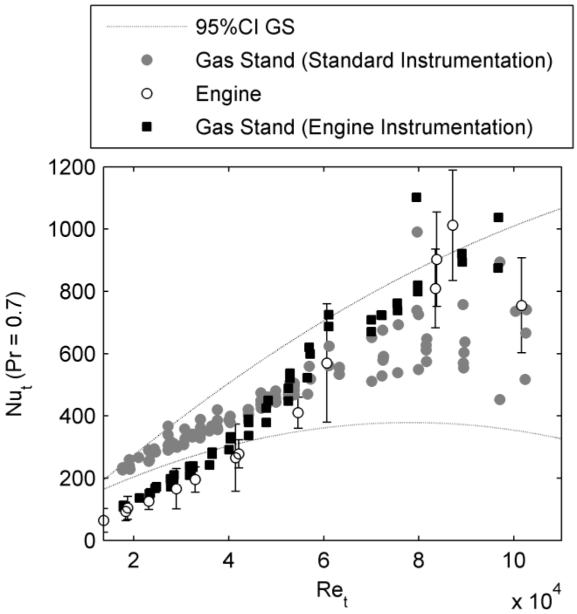

Figure 13: Spatially-Time averaged Nu/Re correlation for engine experiments assuming air and exhaust gases, corrected for Pr=0.7

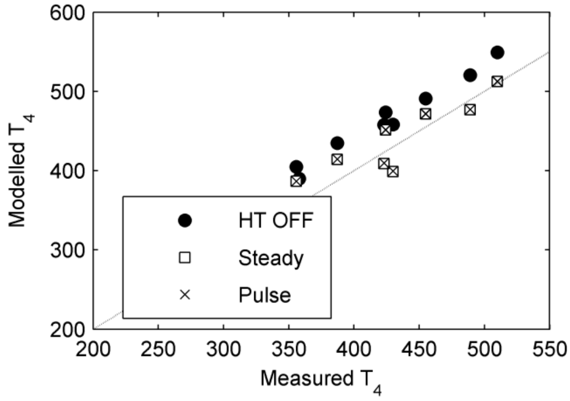

Figure 14: Prediction of turbine outlet temperature without heat transfer, using Spatially-Time-averaged Reynolds number and using Spatially-averaged instantaneous Reynolds number

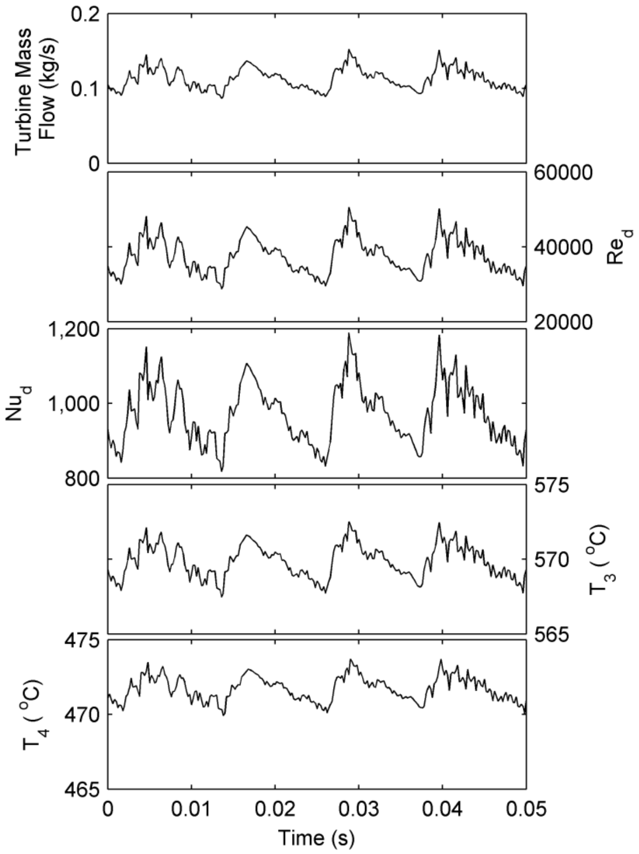

Figure 15: Predicted turbine flow rate, constant gas temperature, instantaneous Reynolds and Nusselt numbers and predicted pulsating turbine outlet temperature

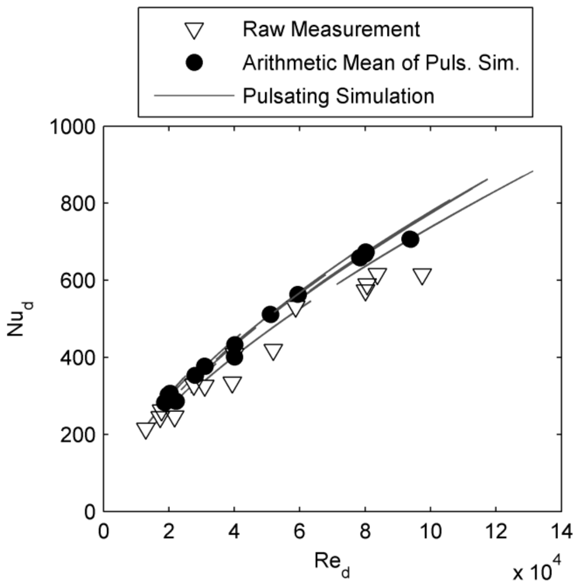

Figure 16: Nusselt/Reynolds relationship for Spatially-Time averaged Reynolds number and spatially averaged instantaneous Reynolds number

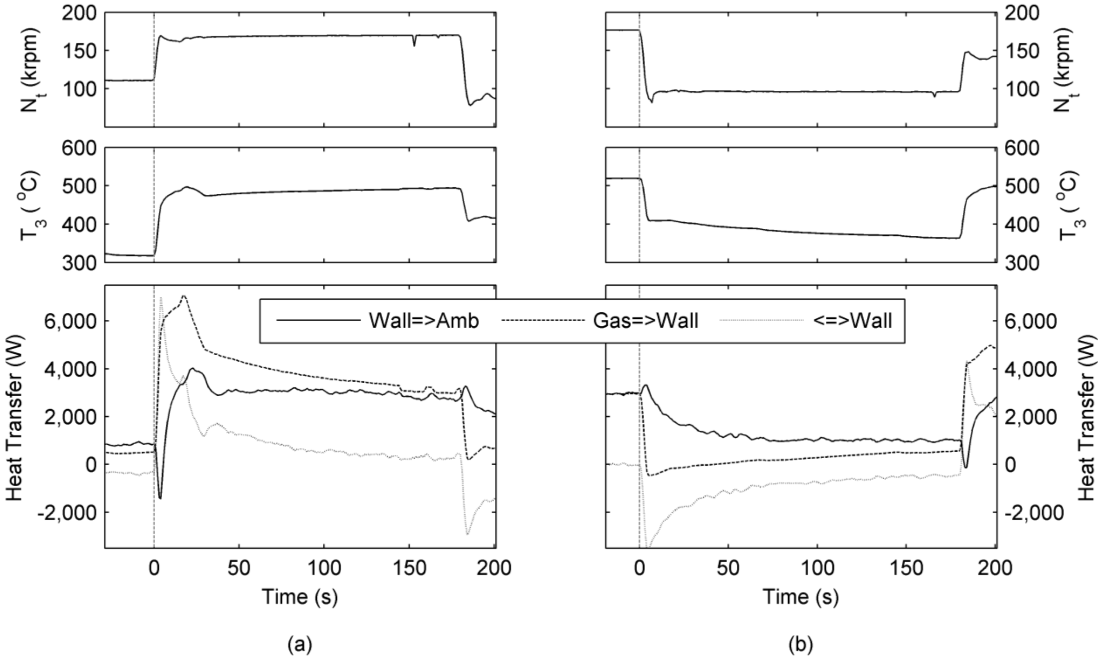

Figure 17: Evolution of turbine rotor speed, Turbine inlet temperature and heat flows between wall and ambient, exhaust gas and wall and heat storage in thermal capacitance of housing during (a) step up in engine power and (b) step down in engine power (0 on the x axis indicates the beginning of each transient)

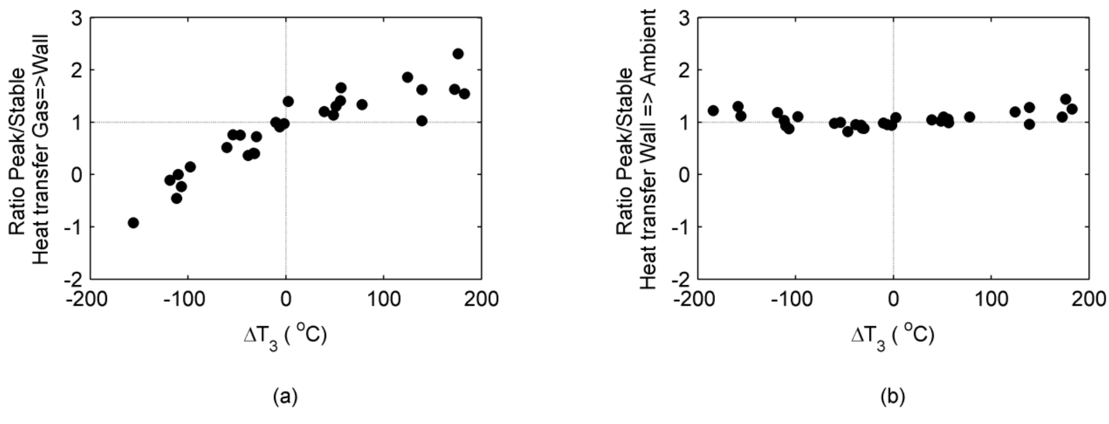

Figure 18: Quotient of Peak transient heat flow to settled heat flow between (a) exhaust gas and turbine housing and (b) turbine housing and ambient

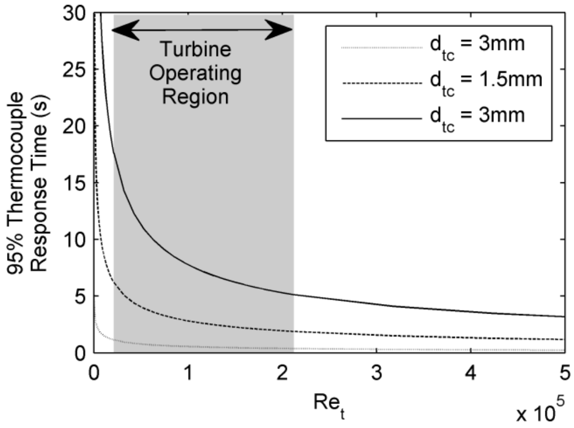

Figure 19: Estimated Thermocouple 95% response time for thermocouple diameters 0.5mm to 3mm as a function of turbine Reynolds number